Title	Efficient Implementation and Design of A New Single-Channel Electrooculography-based Human-Machine Interface System
Author(s)	WU, J; ANG, MS; Tsui, KM; Wu, HC; Hung, YS; Hu, Y; Mak, JNF; Chan, SC; Zhang, Z
Citation	IEEE Transactions on Circuits and Systems II, 2015, v. 62, issue 2, p. 179-183
Issued Date	2015
URL	http://hdl.handle.net/10722/214168
Rights	Creative Commons: Attribution 3.0 Hong Kong License

Efficient Implementation and Design of a New Single-Channel Electrooculography-Based Human–Machine Interface System

J. F. Wu, A. M. S. Ang, K. M. Tsui, H. C. Wu, Y. S. Hung, Y. Hu, J. N. F. Mak, S. C. Chan, and Z. G. Zhang

***Abstract*—This brief introduces a new and practical human–machine interface (HMI) system based on single-channel electrooculography (EOG) signals. The proposed system uses a consumer wireless recording device to collect EOG and employs new encoding/decoding paradigms to convey users' intentions with EOG from eye movements including blinking and looking up. The simplicity and mobility of the system provides a comfortable and practical solution to HMI. Furthermore, to reduce the hardware complexity and power consumption of the signal processing modules of the EOG-based HMI system, a novel multiplierless implementation is developed, where all the algorithms involved, such as bandpass filtering, wavelet filtering, and support vector machine, can be realized using a limited number of adders and shifters only. Experimental results show that the proposed system offers a simple, practical, and yet reliable EOG-based HMI with low complexity and power consumption.**

***Index Terms*—Electrooculography (EOG), human–machine interface (HMI), multiplierless implementation, support vector machine (SVM), wavelet.**

I. Introduction

To reestablish communication between people who are completely or severely paralyzed with the world is a central research problem in neural engineering [1]. Emerging human–machine interface (HMI) technologies have shown great promise to provide a direct communication path between the human body and external machines without muscle activity by translating physiological signals [mainly, electroencephalography (EEG) and electromyography (EMG)] into control commands. Due to the very low signal-to-noise ratio (SNR) of intention-related physiological features, the performance of many HMI systems is highly dependent on complex signal processing algorithms that are usually difficult to implement efficiently in hardware. A low-power implementation of HMI is desirable so that it could be incorporated in portable or mobile applications, such as mind-controlled wheelchair and unmanned vehicles. Currently, efficient hardware realization of commonly used HMI algorithms is still under active research.

Recently, electrooculography (EOG)-based HMI, which infers users' intention from eye movements, such as blinking and looking up/down/left/right, has emerged as a promising technology [2]–[7]. The advantages of EOG as a control signal for HMI include: 1) EOG can be easily observed from most people who can move their eyes, and the signal patterns are highly consistent; and (2) eye movements are intentional and natural movements that do not introduce uncomfortable experience to users. Therefore, EOG–HMI has been considered as a practical alternative to some conventional EEG-based HMIs such as motor-imagery EEG-based HMI systems that cannot work for specific cohorts [8] and visual-evoked-potentials-based HMIs that can easily fatigue users [9]. However, most existing EOG–HMI systems acquire EOG signals from multiple ($3 \sim 8$) wet and often prewired electrodes placed around the eyes, and the setup is not convenient and user friendly [2]–[5]. More importantly, although signal processing algorithms, such as wavelet filtering and support vector machines (SVMs), are useful for removing noise and improving recognition accuracy of EOG [6], [7], they are usually hardware and power intensive in practice. As a result, most existing EOG–HMI systems only perform very basic signal processing such as moving average [4] or even do not perform any preprocessing operations [2]. This seriously impedes the performance and practical applications of EOG–HMI systems.

To overcome these difficulties in designing practical EOG–HMI systems, a new single-channel EOG–HMI system with efficient hardware implementation is developed in this brief. In the proposed EOG–HMI, EOG signals are recorded from a commercial single-channel EEG/EOG acquisition system, namely, MindWave Mobile Headset (NeuroSky, CA, USA), and the user's intention is encoded by combinations of eye movements. The headset places only one dry electrode on the forehead of the user to record mixed EEG/EOG activities and transmits signals to a computer or other hardware system via Bluetooth. Hence, the EOG–HMI equipped with the MindWave Mobile Headset is easy to use and has high mobility.

Furthermore, this brief developed a new encoding/decoding paradigm and a hardware efficient system, which work in tandem with the MindWave Mobile Headset in the EOG–HMI system. Since the headset used in our system places one dry electrode on the skin surface without any conductive gel in-between and any fixed attachment, the noise level of EOG recorded by this headset appears to be relatively higher than that collected by conventional wet electrodes. Therefore, the

Manuscript received June 16, 2014; revised August 19, 2014 and October 13, 2014; accepted November 1, 2014. Date of publication November 7, 2014; date of current version February 7, 2015. This work was supported by a GRF Grant (HKU 785913M) from Hong Kong Research Grants Council. This brief was recommended by Associate Editor R. Rieger. *(J. F. Wu, A. M. S. Ang, and K. M. Tsui contributed equally to this work.) (Corresponding authors: S. C. Chan and Z. G. Zhang.)*

J. F. Wu, A. M. S. Ang, K. M. Tsui, H. C. Wu, Y. S. Hung, S. C. Chan, and Z. G. Zhang are with the Department of Electrical and Electronic Engineering, The University of Hong Kong, Pokfulam, Hong Kong (e-mail: scchan@eee.hku.hk; zgzhang@eee.hku.hk).

Y. Hu is with the Department of Orthopaedics and Traumatology, The University of Hong Kong, Sandy Bay, Hong Kong.

J. N. F. Mak is with the NeuroSky Hong Kong Research Laboratory, Kowloon, Hong Kong.

Digital Object Identifier 10.1109/TCSII.2014.2368617

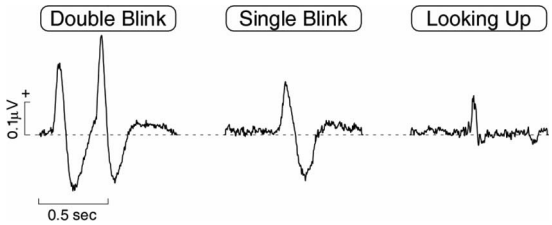

Fig. 1. Three types of EOG signals used in the proposed HMI system.

proposed system performs three different functions: preprocessing (bandpass filtering and wavelet filtering), feature extraction, and classification (SVM), to translate encoded EOG into recognizable commands for external devices. While the accuracy and reliability of these functions are always important for an HMI, particular emphasis has been paid to their implementation complexity and, hence, power consumption to facilitate its efficient implementation on any portable devices. For example, it can be conveniently attached to wheelchairs so that the digital commands decoded could control the movement of the wheelchairs, etc. More precisely, we aim to replace all the expensive multipliers involved in our algorithms, such as filtering, wavelet denoising, SVM, and so on, with hardwired shifters and adders. Such multiplierless realization naturally leads to efficient field-programmable gate array (FPGA) implementation, which generally requires lower hardware cost and consumes less power than direct implementation with a considerable number of general-purpose multipliers. A similar idea also applies to application-specific integrated circuit (ASIC) or very-large-scale integration (VLSI) hardware implementations, where the size and power consumption can be further optimized with dedicated hardware design. Therefore, the resulting low-power and hardware-efficient architecture could generally benefit many other similar wireless body sensor systems. For example, it can be integrated with other lightweight and low-power portable devices, which are used to remotely control other smart home appliances. To demonstrate the usefulness and feasibility of the proposed approach, a system prototype is implemented and tested on Xilinx Zynq XC7Z020 FPGA. Simulation results show that the proposed system offers an attractive mean to realize a simple and reliable HMI with low implementation complexity and power consumption.

II. Single-Channel EOG-Based HMI

A. Encoding Paradigm

The proposed EOG-based HMI system records a single-channel EOG signal with a MindWave Mobile Headset. A user will encode his/her intentions with three different eye movements: double blinking (DB), single blinking (SB), and looking up (LU). The typical EOG signals are shown in Fig. 1.

To enhance the versatility of the system, the command inputted by the user is divided into two parts: 1) DB is used to indicate the start of a new control signal; and 2) a combination of one and/or two eye movements in a 2-s window after DB in 1) is used to encode the control commands. In the present study, we will consider four different combinations including 1) $\langle \mathrm{SB} + \mathrm{LU} \rangle$: one SB followed by one LU, 2) $\langle \mathrm{LU} + \mathrm{SB} \rangle$: one LU followed by one SB, 3) $\langle \mathrm{SB} \rangle$: only one SB, and 4) $\langle \mathrm{LU} \rangle$: only one LU. It should be noted that we have tried several different encoding schemes based on different EOG activities and their combinations. The abovementioned encoding scheme can achieve a good tradeoff between accuracy and control difficulty and, thus, is adopted in this system.

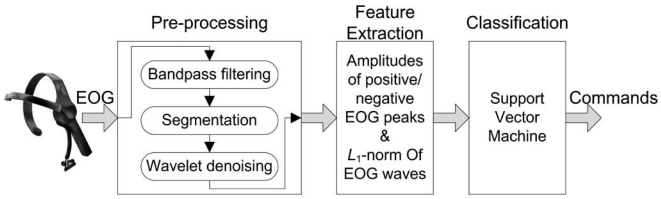

Fig. 2. Diagram of the EOG–HMI system.

B. Decoding Paradigm

To translate encoded EOG signals into digital commands that can be recognized by external devices, the decoding module of the proposed system has three major functions: 1) preprocessing, which includes three steps: bandpass filtering, segmentation, and wavelet denoising, 2) feature extraction, and 3) classification. Fig. 2 shows the block diagram of the whole system. The details of the three decoding functions will be introduced in the following section, along with their efficient hardware implementation.

C. Experimental Design

In the experimental study, subjects were seated in a comfortable chair in an unshielded laboratory with reasonable activities to simulate a real-life situation. EOG signals were continuously recorded using the MindWave Mobile Headset with a sampling rate of 512 Hz. The experiment consisted of two sessions with the same experimental design: The first session is used for training the classifier, and the second session is used for testing the classifier. In each session, the subject was instructed to gaze at the center of a monitor with a viewing distance of 100 cm where the command (one of the four possible commands) was randomly presented. Immediately after seeing the command, the subject did a double-blink and then the corresponding eye movements as indicated by the command. Each control command was presented for 15 times, and the time interval between two consecutive commands is 5 s. The signals recorded in the first session were processed to train a classifier for recognition of commands at a later stage. The classifier and associated hyperparameters were then written to the FPGA board to test the online performance of the proposed system in the second session. All subjects gave their written informed consent, and the local ethics committee approved the experimental procedures.

III. Multiplierless Implementation

In what follows, we shall describe the detail of the three decoding functions and their multiplierless realization.

A. Preprocessing

1) Bandpass Filtering: To remove undesirable noise such as low-frequency drift, high-frequency EEG, and muscle

activities, EOG signals are first bandpass filtered at a bandwidth of 0.5–30 Hz. Without loss of generality, a standard digital bandpass filter (BPF) is used in this work. We note that such filter with fixed coefficients can be realized without any multipliers using sum-of-power-of-two (SOPOT) representation, which will be discussed in Section III-A3. However, details are omitted due to page limitations.

2) Segmentation: From continuous EOG recording, an online detection will be performed to find any DB action, which indicates the onset of a control command encoded in the subsequent 2 s. As seen in Fig. 1, a simple peak detector can be used to detect whether the signal contains two positive peaks in a short time period (1 s). Once DB is detected, the SB or LU will be detected in the subsequent 2 s. Since it is very likely that the duration of both SB and LU activities would not exceed 1 s, we employ a simple peak detector to differentiate any potential candidate activity from background noise. This process is repeated for a sliding window until a suspected eye activity is detected. Then, we perform feature extraction and employ an SVM for classification if the activity found in the data segment belongs to SB or LU. After that, we continue the peak detection and invoke another SVM to classify the second potential candidate, if any, before the end of the 2-s window. We can see that the four-class classification problem can be simplified to two separate binary classification problems. More details on the classifier will be discussed in Section III-C.

3) Wavelet Denoising: To improve SNR and classification accuracy, wavelet denoising is performed on data segments. More precisely, it will be hierarchically decomposed into a series of lower resolution components using discrete wavelet transform (DWT). Next, the DWT coefficients that are smaller than an appropriate threshold (which can be well trained offline) are set to zero. Finally, the data segment will be reconstructed from the thresholded DWT coefficients using inverse DWT (IDWT).

DWT can be performed by iterating a two-channel perfect reconstruction (PR) filter bank (FB) on its lowpass output, and the IDWT is an inverse operation that reconstructs the signal based on its synthesis bank. An efficient implementation structure of the class of biorthogonal FIR PR FBs is called lifting structure [10], which allows fast implementation of the FBs or the WTs because it makes use of similarities between the highpass and lowpass filters to speed up the calculation. One famous example of lifting structured FB commonly used in image compression is the 9/7 FB [11]. Fig. 3 shows a general lifting structure, which is parameterized by two scaling constants C_0 and C_1, and M lifting coefficients p_m, $m = 0, 1, \ldots, M-1$. Moreover, the z-transforms of the analysis filter pairs $[H_0(z), H_1(z)]$ and synthesis filter pairs $[F_0(z), F_1(z)]$ in the lifting structure can be written as

$$H_0(z) = C_0 H^{(M-2)}(z) \text{ and } H_1(z) = C_1 H^{(M-1)}(z) \quad (1)$$

$$F_0(z) = H_1(-z) \text{ and } F_1(z) = -H_0(-z). \quad (2)$$

where $H^{(0)}(z) = z^{-1} + p_0 Q(z^2)$ and $H^{(m)}(z) = z^{-2} H^{(m-2)}(z) + p_m Q(z^2) H^{(m-1)}(z)$ with $Q(z) = (1 + z^{-1})/2$ and $H^{(-1)}(z) = 1$ for $m = 1, 2, \ldots, M-1$. An important advantage of the lifting structured FB is that C_0, C_1, and p_m can be arbitrarily quantized without affecting the PR condition.

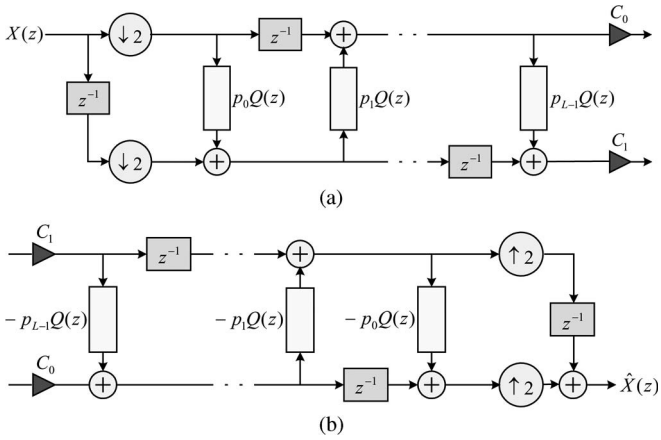

Fig. 3. Lifting structure. (a) Analysis bank (forward transform). (b) Synthesis bank (inverse transform).

TABLE I
SOPOT COEFFICIENTS OF THE 9/7 FB

	9/7 filter bank [11]	SOPOT representation
p_0	-3.17226868408289	$-2^1-2^0-2^{-3}-2^{-5}-2^{-6}-2^{-12}-2^{-13}$
p_1	-0.10596023714940	$-2^{-3}+2^{-6}+2^{-8}-2^{-11}$
p_2	1.76582215102264	$2^1-2^{-2}+2^{-6}+2^{-13}+2^{-14}+2^{-16}$
p_3	0.88701370409649	$2^0-2^{-3}+2^{-7}+2^{-8}+2^{-12}+2^{-15}+2^{-16}$
C_0	0.81289306611600	$2^{-1}+2^{-2}+2^{-4}+2^{-12}+2^{-13}+2^{-15}$
C_1	0.61508705245638	$2^{-1}+2^{-3}-2^{-7}-2^{-9}-2^{-13}-2^{-15}$

We can see that the two basic denoising functions, bandpass filtering and WT, involves a considerable number of multipliers, which are hardware and power intensive. For efficient hardware implementation, we explore the fact that all multipliers involved are constant, and hence, they can be expressed as SOPOT or canonical signed digit [12]. Consequently, expensive multipliers can be replaced with adders and shifters only, leading to multiplierless realization. More precisely, suppose that these multipliers or coefficients are in the following SOPOT representation:

$$\lambda = \sum_{k=0}^{L-1} a_k \cdot 2^{b_k} \quad (3)$$

where λ denotes the approximation of one of the fixed coefficients in either the BPF or DWT (i.e., p_m, C_0, and C_1), L is the number of terms used in the coefficient approximation, $a_k \in \{-1, 0, 1\}$, $b_k \in \{-l_k, \ldots, -1, 0, 1, \ldots, u_k\}$, and l_k and u_k determine the dynamic range of each filter coefficient. The larger the numbers L, l_k, and u_k, the more accurate the SOPOT approximation will be. In practice, the number of nonzero terms is usually kept to a small number, while satisfying given specifications, so that each multiplication can be implemented as limited number of shifts and additions (or subtractions). As an example, Table I summarizes the SOPOT coefficients of the lifting structured FB, which are determined by the algorithm proposed in [13]. We now present the proposed architecture to realize the multiplication with a SOPOT coefficient, which can be variable. Fig. 4 shows such a structure for multiplying an input with a SOPOT coefficient. The proposed structure, which is simply called the S-Unit, consists of two basic modules, namely, a scalable shifter and a variable shifter, which provide

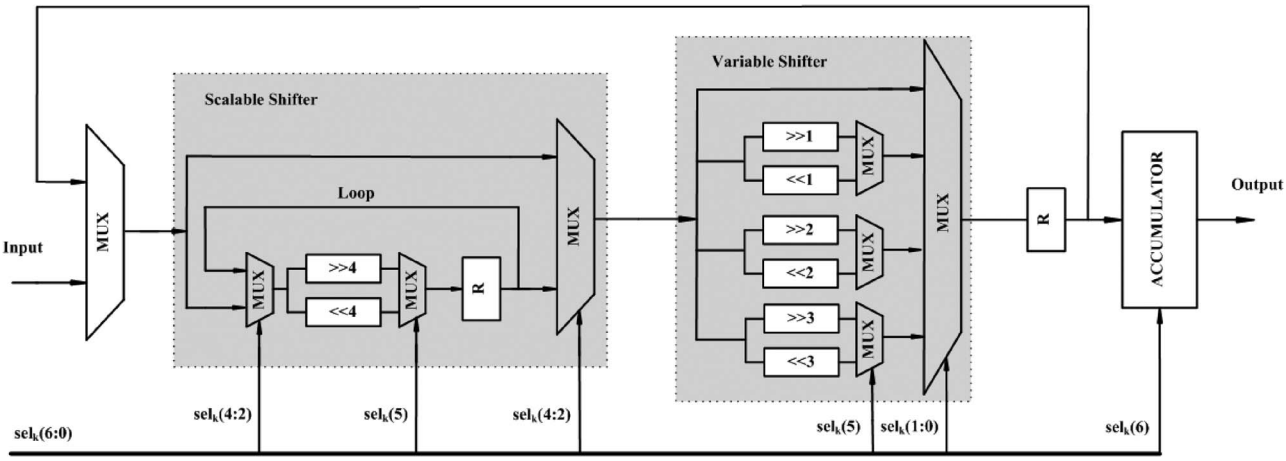

Fig. 4. Proposed structure of an SOPOT unit.

TABLE II
CONFIGURATIONS OF THE CONTROL REGISTERS FOR THE SECOND LIFTING COEFFICIENT p_1 OF DWT

SOPOT Term	Control Register	Configuration
-2^{-3}	sel_0	1100011
2^{-6}	sel_1	0100011
2^{-8}	sel_2	0100010
-2^{-11}	sel_3	1100011

the required shift for a SOPOT term and an accumulator unit, which accumulates the partial sum of SOPOT terms. Two registers, denoted by R, are also used to store the intermediate results. The purpose of decomposing the given shift by a series of fixed and larger shifts and a final stage of small variable shift is to avoid using a programmable shift with a large shifting range, which may consume large hardware resources. In particular, the fixed shift is up to 4 bits, whereas the variable shifter offers variable shift up to 3 bits (both to the left and right). For each SOPOT term $a_k 2^{b_k}$, the exact operation of the S-Unit is controlled by a 7-bit control register $\mathbf{sel_k}$, which specifies the sign of a_k in $\mathbf{sel}_k(6)$, the polarity of shifting direction, i.e., the sign of b_k, in $\mathbf{sel_k}(5)$, the number of rounds used to realize the smallest factor of 4, i.e., $\lfloor |b_k|/4 \rfloor$, in $\mathbf{sel_k}(4..2)$, and the remaining amount of shift, i.e., $|b_k| \bmod 4$, in $\mathbf{sel_k}(1..0)$. Hence, the overall coefficient λ in (3) can be computed by reusing one S-Unit L times with the help of an accumulator. Note that, starting from input with zero shift, the SOPOT terms will be accumulated either in increasing order of their shifts (left and then right) so that only the incremental shift is required at each stage. As an example, $p_1 = -2^{-3} + 2^{-6} + 2^{-8} - 2^{-11}$ can be implemented in four cycles by shifting the input to the right by 3 bits, accumulate; then to the right by 3 bits again, accumulate; two bits to the right, accumulate; and finally, 3 bits to the right and accumulate. Table II shows the configurations of the second lifting coefficient p_1 of the lifting structured FB. Configurations for other SOPOT coefficients can be derived similarly. However, details are omitted due to page limitations.

B. Feature Extraction

As mentioned earlier, we need to classify four combinations of actions, namely, $\langle \mathrm{SB} + \mathrm{LU} \rangle$, $\langle \mathrm{LU} + \mathrm{SB} \rangle$, $\langle \mathrm{SB} \rangle$, and $\langle \mathrm{LU} \rangle$. Therefore, once the signal is filtered, segmented, and denoised as described in Section III-A, several discriminative features should be chosen to enhance the classification accuracy of differentiating SB and LU. According to Fig. 1, we find that the following three features: 1) amplitude of positive peak, 2) amplitude of negative peak, and 3) L_1-norm of EOG waveforms are effective in discriminating SB and LU while their computations do not require too much hardware cost. Due to page limitations, details are omitted here.

C. Classification (SVM)

To classify the extracted features, we first standardize the three features, x_j^{test}, $j = 1,2,3$, as

$$\bar{x}_j^{\mathrm{test}} = \left(x_j^{\mathrm{test}} - \mu_j\right)/\sigma_j \tag{4}$$

where μ_j and σ_j denote the corresponding mean and standard deviation, respectively. Then, the following linear classification or decision rule is used to classify the extracted feature and normalized feature $\bar{\boldsymbol{x}}^{\mathrm{test}}$:

$$\begin{cases} \hat{y} = 1, & \boldsymbol{w}^T \bar{\boldsymbol{x}}^{\mathrm{test}} - b \geq 0 \\ \hat{y} = -1, & \text{otherwise} \end{cases} \tag{5}$$

where $\hat{y}$ denotes the estimated class label for either SB or LU, $\bar{\boldsymbol{x}}^{\mathrm{test}}$ denotes the standardized feature vector with its jth value given in (4), and $\boldsymbol{w}$ and b denote the parameter of the SVM under consideration. To simplify the decoder hardware implementation, we assume that μ_j and σ_j in (4) and $\boldsymbol{w}$ and b in (5) have been precomputed from the training data of each user. In particular, the latter can be determined by solving the following optimization problem [14]:

$$\begin{cases} \min\limits_{\boldsymbol{w},b,\xi_t} & 0.5\,\|\boldsymbol{w}\|_2^2 + C\sum_{\forall t \in \Omega} \xi_t \\ \text{s.t.} & y_t(\boldsymbol{w}^T \bar{\boldsymbol{x}}_t - b) \geq 1 - \xi_t \text{ and } \xi_t \geq 0,\ \forall t \in \Omega \end{cases} \tag{6}$$

where Ω denotes the training data set. Note the term $C\sum_{\forall t \in \Omega} \xi_t$ is called the soft margin, which is used to deal with possible mislabeled samples, and the associated parameter C can be chosen by cross-validation of the training samples. Since μ_j, σ_j, $\boldsymbol{w}$, and b are fixed, they can again be represented in the form of SOPOT coefficients in (3). Hence, the classification in (5) can be similarly implemented without any multipliers.

TABLE III
SENSITIVITY AND SPECIFICITY FOR EACH CLASS OF SIX SUBJECTS

	<SB>	<LU>	<SB+LU>	<LU+SB>
Sensitivity	93.06±11.08%	79.58±27.41%	80.34±22.11%	84.63±12.05%
Specificity	96.59±5.64%	99.12±2.18%	97.68±4.24%	88.62±7.17%

TABLE IV
SAVINGS OF HARDWARE COMPLEXITY AND POWER CONSUMPTION FOR THE PROPOSED MULTIPLIERLESS ARCHITECTURE

	Before SOPOT		After SOPOT	
	LS	NP	LS	NP
BPF	2896	2.01	1229	1.05
DWT	11903	7.21	4792	4.02
Total	17292	10.95	8288	6.38

LS: Logic Slices; NP: Normalized Power (mW)

IV. EXPERIMENTAL RESULTS

Experimental results on six subjects (years: 30.8 ± 13.5; 1 female) showed that the accuracy for classifying four classes is $92.30 \pm 4.72\%$ from processed data and $88.04 \pm 2.82\%$ from raw data. Statistical test showed that the proposed signal processing steps can significantly improve the classification accuracy ($p = 0.027$, paired sample t-test). Table III further showed the sensitivity and specificity for each class.

The performance of the HMI system was also assessed using the information transfer rate (ITR), i.e.,

$$ITR = L \cdot \left[p \log_2(p) + (1-p) \log_2 \left(\frac{1-p}{N-1} \right) + \log_2(N) \right] \tag{7}$$

where $L = 12$ is the number of decisions in 1 min, and $p = 92.30\%$ is the accuracy of subjects in making decisions among $N = 4$ targets. Thus, the ITR of the EOG-based HMI system was 17.84 bits/min. Since the number of eye movements that can be detected by the proposed system is limited by the single-channel device, the ITR of the system may not be as high as some EOG–HMI systems based on multiple electrodes or multimodalities [4]. Nevertheless, it is still sufficient for basic communication and control functions [1].

The proposed architecture is implemented and tested on the Xilinx Zynq XC7Z020 FPGA [15]. All components in the proposed multiplierless structures are specified using Verilog. The compilation and simulation were done using the ISE Design Suite 14.7 from Xilinx Corporation [16]. The hardware complexity in terms of number of logic slices (LS) used and the normalized power consumption [17] at a 50-MHz clock frequency of the main components are summarized in Table IV, where we also demonstrate the two most expensive components, namely, BPF and DWT, that require the most LS. In general, we can see that the proposed multiplierless architecture requires less hardware complexity and achieves lower power consumption than the direct implementation using general-purpose multipliers. It is expected that more savings in hardware complexity and power consumption can be achieved in ASIC or VLSI realization.

V. CONCLUSION

The architecture and multiplierless implementation of a new EOG-based HMI system using SOPOT representation have been presented. Experimental results show that the proposed EOG–HMI system offers satisfactory performance in terms of classification accuracy, implementation complexity, and power consumption. Compared with existing EOG–HMI systems, the proposed system has a very simple system setup (based on a consumer user-friendly wireless EEG device) and is able to achieve good performance due to the multiplierless realization of complicated signal processing methods. This suggests that the proposed system may be an attractive alternative to existing HMI systems in healthcare applications such as therapy. In addition, the low-power and hardware-efficient architecture could benefit many other applications involving filtering, denoising, and classification. In future work, we will further optimize the encoding/decoding scheme, with the aim to provide a reliable and user-friendly HMI system. In particular, we shall focus on several important design factors (such as time to learn, cost effectiveness, short- and long-term reliability, subjective satisfaction, etc.) in order to facilitate its practical applications.

REFERENCES

[1] J. R. Wolpaw, N. Birbaumer, D. J. McFarland, G. Pfurtscheller, and T. M. Vaughan, "Brain–computer interfaces for communication and control," *Clin. Neurophysiol.*, vol. 113, no. 6, pp. 767–791, Jun. 2002.

[2] Y. Punsawad, Y. Wongsawat, and M. Parnichkun, "Hybrid EEG-EOG brain–computer interface system for practical machine control," in *Proc. IEEE Conf. EMBS*, 2010, pp. 1360–1363.

[3] E. English, A. Hung, E. Kesten, D. Latulipe, and Z. P. Jin, "EyePhone: A mobile EOG-based human–computer interface for assistive healthcare," in *Proc. IEEE Conf. EMBS NER*, 2013, pp. 105–108.

[4] S. L. Wu *et al.*, "Controlling a human–computer interface system with a novel classification method that uses electrooculography signals," *IEEE Trans. Biomed. Eng.*, vol. 60, no. 8, pp. 2133–2141, Aug. 2013.

[5] Y. Nam, B. Koo, A. Cichocki, and S. Choi, "GOM-Face: GKP, EOG, EMG-based multimodal interface with application to humanoid robot control," *IEEE Trans. Biomed. Eng.*, vol. 61, no. 2, pp. 453–462, Feb. 2014.

[6] T. Yagi, Y. Kuno, K. Koga, and T. Mukai, "Drifting and blinking compensation in electro-oculography (EOG) eye-gaze interface," in *Proc. IEEE Conf. SMC*, 2006, pp. 3222–3226.

[7] A. Bulling, J. A. Ward, H. Gellersen, and G. Troster, "Eye movement analysis for activity recognition using electrooculography," *IEEE Trans. Pattern. Anal. Mach. Intell.*, vol. 33, no. 4, pp. 741–753, Apr. 2011.

[8] C. Vidaurre and B. Blankertz, "Towards a cure for BCI illiteracy," *Brain Topogr.*, vol. 23, no. 2, pp. 194–198, Jun. 2010.

[9] Y. H. Tu, Y. S. Hung, G. Huang, L. Hu, and Z. G. Zhang, "An automated and fast approach to detect single-trial visual evoked potentials with application to brain–computer interface," *Clin. Neurophysiol*, vol. 125, no. 12, pp. 2372–2383, Dec. 2014.

[10] W. Sweldens, "The lifting scheme: A new philosophy in biorthogonal wavelet construction," in *Proc. SPIE*, 1995, vol. 2569, pp. 68–79.

[11] A. Cohen, I. Daubechies, and J. C. Feauveau, "Biorthogonal bases of compactly supported wavelets," *Commun. Pure Appl. Math.*, vol. 45, no. 5, pp. 485–560, Jun. 1992.

[12] Y. C. Lim and S. R. Parker, "FIR filter design over a discrete power-of-two coefficient space," *IEEE Trans. Acoust., Speech, Signal Process.*, vol. ASSP-31, pp. 583–591, Apr. 1983.

[13] S. C. Chan, K. M. Tsui, K. S. Yeung, and T. I. Yuk, "Design and complexity optimization of a new digital IF for software radio receivers with prescribed output accuracy," *IEEE Trans. Circuits Syst. I, Reg. Papers*, vol. 54, no. 2, pp. 351–366, Feb. 2007.

[14] C. Cortes and V. Vapnik, "Support-vector networks," *Mach. Learn.*, vol. 20, no. 3, pp. 273–297, 1995.

[15] Zynq XC7Z020. [Online]. Available: http://www.xilinx.com/support/documentation/data_sheets/ds187-XC7Z010-XC7Z020-Data-Sheet.pdf

[16] ISE Design Suite. [Online]. Available: http://www.xilinx.com/support/index.html/content/xilinx/en/supportNav/design_tools/ise_design_suite.html

[17] J. H. Yen, L. R. Dung, and C. Y. Shen, "Design of power-aware multiplier with graceful quality–power trade-offs," in *Proc. IEEE ISCAS*, May 2005, vol. 2, pp. 1642–1645.